Wavenumber Sampling Issues in 2.5D Frequency Domain Seismic Modelling

Catherine Sinclair,[1] Stewart Greenhalgh,[1,2] and Bing Zhou[1]

Abstract—There are several important wavenumber sampling issues associated with 2.5D seismic modelling in the frequency domain, which need careful attention if accurate results are to be obtained. At certain critical wavenumbers there exist rapid disruptions in the mainly smooth oscillatory spectra. The amplitudes of these disruptions can be very large, and this affects the accuracy of the inverse Fourier transformed frequency-space domain solution. In anisotropic elastic media there are critical wavenumbers associated with each wave mode—the quasi-P (qP) wave, and the two quasi-shear (qS1 and qS2) waves. A small wavenumber sampling interval is desirable in order to capture the highly oscillatory nature of the wavenumber spectrum, especially at increasing distance from the source. Obviously a small wavenumber sampling interval adds greatly to the computational effort because a 2D problem must be solved for every wavenumber and every frequency. The discretisation should be carried out up to some maximum wavenumber, beyond which the field becomes evanescent (exponentially decaying or diffusive). For receivers close to the source, activity persists beyond the critical wavenumber associated with the minimum shear wave velocity in the model. Fortunately, for receivers well removed from the source, the contribution from the evanescent energy is negligible and so there is no need to sample beyond this critical wavenumber. Sampling at Gauss–Legendre spacings is a satisfactory approach for acoustic media, but it is not practical in elastic media due to the difficulty of partitioning the integration around the different critical wavenumbers. We found to our surprise that in transversely isotropic media, the critical wavenumbers are independent of wave direction, but always occur at those wavenumbers corresponding to the maximum phase velocities of the three wave modes (qP, qS1 and qS2), which depend only on the elastic constants and the density. Additionally, we have observed that intermediate layers between source and receiver can filter out to a large degree, the sharp irregularities around the critical wavenumbers in the ω–k_y spectra. We have found that, using the spectral element method, the singularities (poles) at the critical wavenumbers which exist with analytic solutions, do not arise. However, the troublesome spike-like behaviour still occurs and can be damped out without distorting the spectrum elsewhere, through the introduction of slight attenuation.

1. Introduction

Forward modelling of seismic waves is an essential part of inversion, to elucidate the structure and elastic properties of the subsurface. It is also an indispensable aid to seismic survey design, to the processing and interpretation of seismic field data, and in knowing what type of response to expect for a given geological situation. There are several approaches to simulating seismic wavefields (e.g., finite difference, finite element, spectral element, pseudo-spectral, boundary integral) involving varying degrees of algorithmic and model complexity (Marfurt 1984; Kelly and Marfurt 1990; Bouchon 1996; Komatitsch et al. 2000; Carcione 2007). Modelling in 2.5D offers major computational advantages over full 3D modelling when the subsurface can be adequately approximated with a 2D model, i.e., no variation in material properties in the strike or *y*-direction. Modelling in 2.5D is significantly faster than 3D modelling and uses far less memory. It yields wavefields having point-source like properties (spreading in 3D) as opposed to 2D modelling which carries the implicit assumption of a line source. Modelling in 2.5D entails taking a spatial Fourier transform along the *y*-direction and moving into the wavenumber (k_y) domain. The resulting partial differential equation is then solved by a numerical method (e.g., finite difference, finite element, pseudospectral) essentially as a 2D problem, but for a variety of wavenumbers. The final solution is then reconstructed in the spatial domain by taking an inverse Fourier transform of the wavenumber spectrum.

[1] Department of Physics, University of Adelaide, Adelaide, SA 5005, Australia. E-mail: funklair@hotmail.com; gstewart@aug.ig.erdw.ethz.ch; bing.zhou@adelaide.edu.au
[2] Institute of Geophysics, ETH Zurich, Zurich, Switzerland.

Only a handful of papers have appeared in the literature on true 2.5D modelling. It can be carried out in either the time domain or the frequency domain. STOCKWELL (1995) tackled the acoustic problem in the time domain in an approximate way using asymptotic ray theory and restricted himself to in-plane propagation. RANDALL (1991) and OKAMOTO (1994) presented more elaborate and accurate out-of-plane time domain finite difference 2.5D methods for acoustic and elastic waves in isotropic media, whereas SONG and WILLIAMSON (1995) and CAO and GREENHALGH (1997, 1998) described frequency domain finite difference approaches to the problem in acoustic only media. ZHOU and GREENHALGH (1998a, b, 2006) presented frequency domain finite element acoustic algorithms, while YANG and HUNG (2001) gave a hybrid finite element, infinite element elastic formulation. FURUMURA and TANENAKA (1996) described a pseudo-spectral time domain 2.5D algorithm for elastic media. Boundary integral equation 2.5D modelling for elastic media was described by TANENAKA et al. (1996) and FUJIWARA (1997) Finally, SINCLAIR et al. (2007) solved the 2.5D anisotropic problem in the frequency domain using a spectral element approach.

Frequency domain modelling has some advantages over time domain modelling. Simulating seismic responses in the frequency domain considerably reduces the computational burden in terms of run time, because inversion results can be produced using a limited number of frequency components (PRATT 1990; MAURER et al. 2009). In frequency domain modelling, the suppression of waves within absorbing boundaries is easily achieved via modification of the imaginary part. A further advantage arises when modelling for multiple sources. The time consuming factorization step of LU decomposition (i.e., decomposing a square matrix into lower and upper triangular matrices of equal size) in solving the matrix system of equations only needs to be performed once, thereby reducing computation time for subsequent sources (MARFURT 1984). An additional advantage of frequency domain modelling is the independence of the solutions for each frequency, so the problem is easily run in parallel on a computer cluster. In time domain modelling, explicit time marching schemes are often used to advance the

solution in time. The solution at each time step depends on previous time step solutions. Thus, the solutions can drift from the actual solution as the errors accumulate.

A problem of 2.5D frequency domain modelling is the existence of poles or erratic fluctuations in the wavenumber spectrum for certain critical wavenumbers (ZHOU and GREENHALGH 2006). The problem does not arise in time domain modelling. Almost all of the papers in the literature say very little about the wavenumber sampling mechanism and how to integrate (inverse Fourier transform) through possible singularities in the wavenumber spectrum. They provide very little guidance on the practical aspects of implementation. The paper by SINCLAIR et al. (2007) is possibly the only example where the authors acknowledge the presence of pole-like behaviour close to critical wavenumbers for frequency domain 2.5D elastic wave modelling. ZHOU and GREENHALGH (2006) observed the behaviour in the analytic *acoustic* case but did not have to integrate through the singularity in order to form a frequency domain solution because the acoustic case only involves the *P*-wave mode and for receivers at some distance from the source, there is no contribution from the evanescent field. It was only necessary to integrate up to the critical wavenumber associated with the *P*-wave mode. SINCLAIR et al. (2007) suggest skipping the critical wavenumbers in the wavenumber summation for the elastic case, but this can produce inaccurate solutions, as demonstrated by SINCLAIR (2009).

It seems that most researchers and practitioners in seismic modelling avoid the issue entirely and prefer to use simple 2D (line source) modelling and then construct an approximate 2.5D (point source) solution from this by applying simple filters. These filters correct amplitudes (usually by scaling as $1/\sqrt{r}$, where r is the distance or travel time) and adjust phases (by $\pi/4$) to obtain approximate 2.5D solutions (see BLEISTEIN 1986; LINER 1991). In this way, during an inversion or migration the 2D modelled data can be compared with the actual field data (involving point sources) after the field data has been converted from 3D (or 2.5D) to 2D. However, the filters are only accurate in the far-field in near-constant velocity media, and for single isolated arrivals. It was shown by WILLIAMSON and PRATT (1995), in a critical review

of acoustic modelling, that the errors can become substantial in complex media and where multiple, overlapping arrivals are present. Despite such limitations the pseudo 2.5D method and the 2D method remain popular (mainly because of the simplicity of 2D modelling) and are used in many inversion algorithms (CHOI *et al.* 2008; ROBERTS *et al.* 2008; SEARS *et al.* 2008). Inversion of ground penetrating radar data is also based on 2D modelling and simple corrections to adjust the recorded (2.5D or 3D) data to 2D wavefield characteristics (ERNST *et al.* 2007).

BOUCHON (2003), in a review of the discrete wavenumber method for 1D media, provides several simple acoustic and elastic examples of integrals representing an inverse Fourier transform from the frequency–wavenumber domain to the frequency-space domain, where the integrand is given in explicit analytic form and contains singularities within the range of integration. He suggests discretising the integrand for various wavenumbers k and performing a straight summation, but no suggestion is made as to how the solution is affected if one of the wavenumber samples falls close to or directly on the singularity. Likewise, when considering the 2.5D solution for an isotropic homogeneous full space, TADEU and KAUSEL (2000) do not mention how to circumvent the presence of singularities in their analytic solution for the frequency–wavenumber domain. Their solution involves zero order Hankel functions of the second kind $H_0^2(k_\alpha r)$ and $H_0^2(k_\beta r)$ where $k_\alpha = \sqrt{k_p^2 - k_y^2}$, $k_\beta = \sqrt{k_s^2 - k_y^2}$, with $k_p = \omega$, $k_s = \omega/\beta$, α is the *P*-wave velocity and β is the *S*-wave velocity. The Hankel functions contain singularities when the wavenumber $k_y = k_p$ or $k_y = k_s$. In an earlier paper, FUJIWARA (1996) considers the more general problem of the frequency–wavenumber domain Green's functions for computing the 3D wavefield in a 2D basin structure of arbitrary cross section involving a free surface. The solution was obtained by a boundary element method but no specific mention is made of the critical wavenumbers.

Other less complicated models than a 2D basin structure (e.g., a layer over a half space) have analytic solutions expressed in the form of infinite integrals (EWING *et al.* 1957) where poles occur in the integrand. The usual method of solution for such simple 1D models is to perform a contour integration and to express the solution as the sum of the residues at the poles. It is often difficult to find the correct contour, especially where branch points occur. But for 2D and 3D models no analytic expressions (infinite integrals) exist and solutions can only be obtained numerically, so a different approach is required.

SONG and WILLIAMSON (1995) describe 2.5D numerical modelling for acoustic waves in heterogeneous media but do not mention singularities. To form the inverse spatial Fourier transform, they sample along the wavenumber axis from 0 to slightly beyond the critical wavenumber associated with the *P*-wave ($k_c = \omega/c$), where c is the speed of the *P*-wave near the surface, so they are actually integrating through the singularity.

In this paper we demonstrate how performing blind wavenumber summation through the critical wavenumbers can badly affect the inverse Fourier transformed frequency domain solution. We systematically examine the wavenumber sampling issue for isotropic as well as anisotropic media, and offer some guidance on an effective strategy for 2.5D modelling.

2. *Wavenumber Sampling and the 2.5D Frequency Domain Modelling Method*

We first provide a brief theoretical description of the 2.5D frequency domain modelling method. The 2.5D elastic equation of motion in the frequency domain is given by:

$$-\rho\omega^2\bar{\bar{\mathbf{s}}} = \bar{\nabla} \cdot (\mathbf{c} \mathbin{:} \bar{\nabla}\bar{\bar{\mathbf{s}}}) \qquad (1)$$

where ρ is the density, ω is the angular frequency, $\bar{\bar{\mathbf{s}}} = (\bar{\bar{s}}_x, \bar{\bar{s}}_y, \bar{\bar{s}}_z)$ is the displacement vector and the two bars indicate that the quantity has been temporally Fourier transformed and spatially Fourier transformed in the *y*-direction. The quantity $\bar{\nabla} = (\partial_x, ik_y, \partial_z)$ is the 2.5D gradient vector operator where k_y is the particular wavenumber, and $\mathbf{c}$ is the fourth rank tensor of elastic coefficients. The colon represents the double dot product between the fourth rank elasticity tensor and a second rank tensor (the gradient of the displacement vector) which produces a second rank tensor, $\mathbf{A} \mathbin{:} \mathbf{B} = \hat{\mathbf{i}}\hat{\mathbf{j}}A_{ijkl}B_{kl} = \hat{\mathbf{i}}\hat{\mathbf{j}}D_{ij}$.

A source vector is introduced into the equation of motion and the equations are solved as a series of 2D

problems to obtain $\bar{\bar{\mathbf{s}}}$ for each wavenumber (and frequency). The 2.5D frequency–space domain solution is computed by taking the inverse spatial Fourier transform with respect to k_y:

$$\bar{\mathbf{s}}(\omega, x, y, z) = \frac{1}{2\pi} \int_{\infty}^{\infty} \bar{\bar{\mathbf{s}}}(\omega, x, k_y, z) e^{ik_y y} dk_y$$

$$\approx \frac{\Delta k_y}{2\pi} \sum_j \bar{\bar{\mathbf{s}}}(\omega, x, k_y^j, z) e^{ik_y^j y} \qquad (2)$$

where Δk_y is the spacing between wavenumbers. In the x–z plane containing the source ($y = 0$), Eq. 2 amounts to a simple summation of the 2D frequency–wavenumber domain solutions. Note that the solution for $k_y = 0$ is the 2D modelling result.

The problem of 2.5D frequency domain modelling lies in the choice of a wavenumber sampling strategy. The efficiency of the modelling is dependent on the number of wavenumbers used, because the numerical system of linear equations (e.g., finite element, spectral element) must be solved for every wavenumber (and frequency) value. The computational time increases significantly if the number of wavenumber samples is high.

As illustrated in Eq. 2, it is essential in actual computations that the wavenumber k_y be discretised or sampled at some interval Δk_y. The discretisation in the wavenumber domain corresponds to periodicity in the y domain. The wavenumber periodicity or repetition length is given by $L = 2\pi/\Delta k_y$, and so the finer the sampling, the longer the period. As shown by BOUCHON (2003), the discretisation of the wavenumbers corresponds to solving a multiple source problem where the sources are periodically distributed along the y-axis at spacing L. The contribution from the multiple sources can be attenuated during the inverse Fourier transform in the complex frequency plane via the introduction of a small imaginary part into the frequency. It is important to observe that the smaller we choose Δk_y, the more distant the multiple sources from the receiver and so their contribution is greatly reduced.

For receivers close to the source, the evanescent energy makes a significant contribution to the total wavefield. This energy appears in the frequency–wavenumber domain spectrum as activity beyond the wavenumber ($k_c^S = \omega/V_{Smin}$) associated with the slowest S mode, the so-called cutoff wavenumber. Figure 1 shows the frequency–wavenumber domain spectra of the numerically Fourier transformed analytic solution for an isotropic full-space (AKI and RICHARDS 1980), at several points in the model at distances of 2, 4, 8 and 12 m from the source. The P- and S-wave velocities and the density for the model are those given in Table 1 for medium B. The frequency is 300 Hz. The cut-off wavenumber is 1.57 rad m^{-1}. The plots demonstrate that as the distance from the source increases, the amount of evanescent energy diminishes in comparison to the propagation energy. For increased accuracy in the inverse Fourier-transformed frequency domain solution at receivers close to the source, the evanescent energy should be included by sampling beyond the cutoff wavenumber.

It has been observed in *acoustic* wave modelling, that in the frequency–wavenumber domain, the frequency of oscillations increases with increasing wavenumber and with increasing distance from the source (ZHOU and GREENHALGH 2006). This behaviour is also apparent in *elastic* wave modelling as demonstrated in Fig. 2 for the numerically Fourier transformed analytic solution for an elastic isotropic full-space (AKI and RICHARDS 1980) having the properties of medium A listed in Table 1. Each plot shows the frequency–wavenumber domain solution at separate points in the model, at distances of 7.5, 15, 30 and 60 m from the source.

For acoustic modelling, an efficient wavenumber sampling strategy has been developed using Gauss–Legendre integration to exploit the increasingly oscillatory behaviour of the frequency–wavenumber domain Green's function solutions (CAO and GREENHALGH 1998, ZHOU and GREENHALGH 2006). Using Legendre spacings, the sampling rate at lower wavenumbers is lower than at higher wavenumbers, thereby reducing the total number of samples required compared to an equal sampling interval. The Nyquist requirement of at least two samples per wavelength is obeyed and aliasing is avoided.

ZHOU and GREENHALGH (2006) observed disruptive behaviour in the wavenumber spectra as the wavenumber approached a singular value associated with the P-wave mode. They avoided sampling too close to the critical wavenumber. In the elastic isotropic
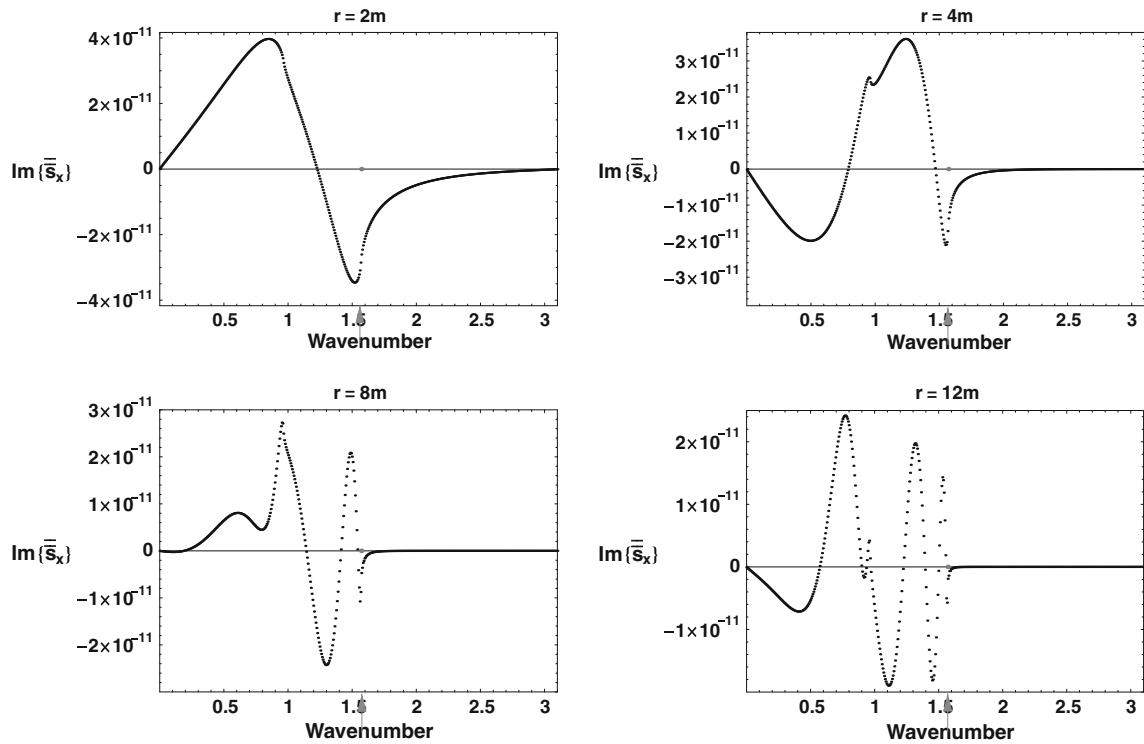
Figure 1

At small distances from the source the evanescent energy persists beyond the cutoff wavenumber (indicated by the *grey arrows* at 1.57 rad m^{-1}). The medium is homogeneous and isotropic medium B as described in Table 1. The frequency is 300 Hz. The receivers are placed horizontally from the source at 2, 4, 8 and 12 m distances. The source is real and *y*-directed. The *P*-wave critical wavenumber is 0.97 rad m^{-1}

Table 1

Properties of isotropic media A and B

Medium	Elastic coefficients	Group/phase velocities (km/s)	Critical wavenumbers
A	$A_{33} = 6.30$, $A_{44} = 1.00$	$P = 2.50998$, $S = 1.00000$	0.75, 1.89
B	$A_{33} = 3.8025$, $A_{44} = 1.00$	$P = 1.95000$, $S = 1.20000$	0.97, 1.57

The elastic moduli A_{ii} ($=C_{ii}/\rho$) listed above are density-normalised

case, the situation is more complicated than in the acoustic case because there are two wave modes (*P* and *S*) to consider and hence two critical wavenumbers, as indicated in Figs. 1 and 2. To produce an accurate inverse Fourier transformed frequency domain solution in the numerical case, it is necessary to integrate through the first critical wavenumber. For anisotropic media, the situation is even worse where there are three modes of propagation (qP, qS$_1$, qS$_2$) and a directional dependence in velocity (and hence possibly in the critical wavenumber values).

3. *Observations of Critical Wavenumbers*

In the acoustic case, the apparent wavenumber observed in the *x*–*z* plane for a particular frequency–wavenumber domain solution is given by: $k_a = \sqrt{k^2 - k_y^2}$ where k_a is the apparent wavenumber and $k = \omega/c$ is the actual wavenumber, where *c* is the medium velocity (ZHOU and GREENHALGH 2006). When k_y approaches k, the apparent wavenumber approaches zero, causing disruptions to the
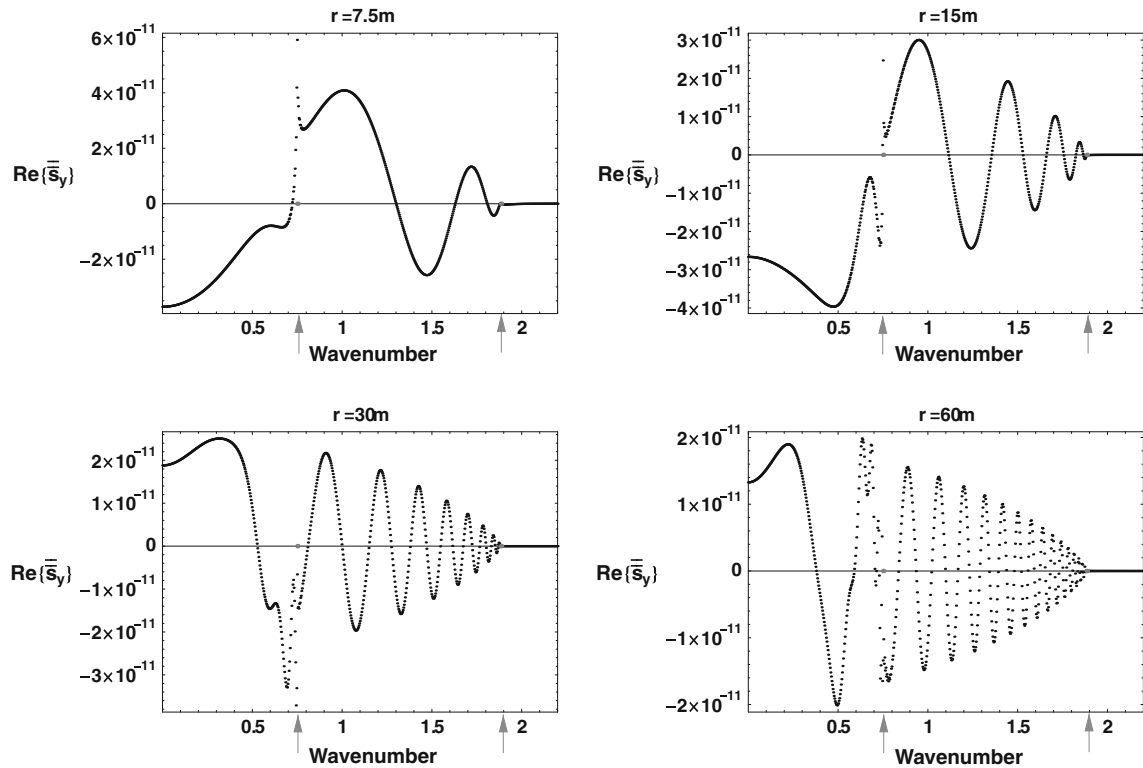
Figure 2

The frequency–wavenumber domain Fourier transformed analytic solutions exhibit increasingly oscillatory behaviour as the distance between source and receiver is increased. For a particular distance, as the wavenumber increases, the frequency of oscillation also increases. The real y component of the solution for 1,024 equally spaced wavenumbers is shown. Receivers are placed at distances $r = 7.5, 15, 30$ and 60 m from the source. The source is y-directed. The frequency is 300 Hz. The medium is homogeneous isotropic medium A from Table 1. The critical wavenumbers at 0.751 and 1.885 rad m^{-1} are indicated in *grey*

frequency–wavenumber domain solutions, so k_y is said to be approaching a *critical* wavenumber.

In the homogeneous isotropic elastic full space there are two critical wavenumbers $(k_y^c)_P$ and $(k_y^c)_S$, which are associated with the longitudinal (*P*-wave) and transverse (*S*-wave) modes via:

$$(k_y^c)_P = \omega/V_P, \quad (k_y^c)_S = \omega/V_S$$

where ω is angular frequency and V_P and V_s are the *P*-wave and *S*-wave velocities, respectively.

Figure 3 shows the real part of a numerically calculated 2.5D frequency–wavenumber domain spectrum at a single point (distance 33 m from the source) for a homogeneous isotropic elastic full space, using medium B from Table 1. The numerical method used to calculate the spectra was the spectral element method (SINCLAIR *et al.* 2007). A disruption is visible at the approximate wavenumber value of

0.97 rad m^{-1} and propagation continues up until wavenumber 1.57 rad m^{-1}, the cutoff wavenumber. The properties of the medium relevant to the calculation of the critical wavenumbers are also shown in Table 1.

Figure 4 shows results for a homogeneous vertically transversely isotropic (VTI) full space. The density normalised coefficients $A_{ij} = C_{ij}/\rho$ for the medium are listed in the figure caption. The plotted quantity is the real component of the doubly Fourier transformed y-component of displacement for a y-directed source. In this medium we observe two disruptions in the spectrum at wavenumbers 0.75 and 1.10 rad m^{-1}, as well as a cutoff point at wavenumber 1.89 rad m^{-1}. In a VTI medium the critical wavenumbers are associated with the three wave modes—the quasi-P (*P*-wave), quasi-S1 (SV-wave) and the quasi-S2 (SH-wave) modes.
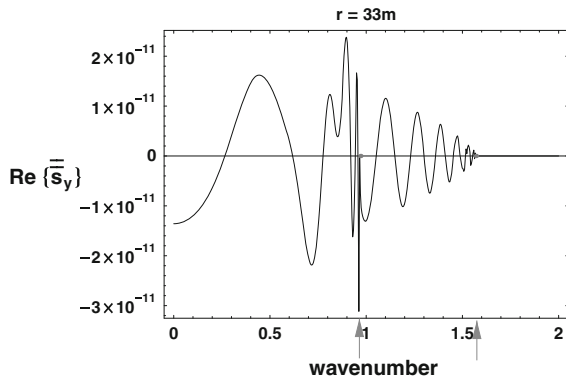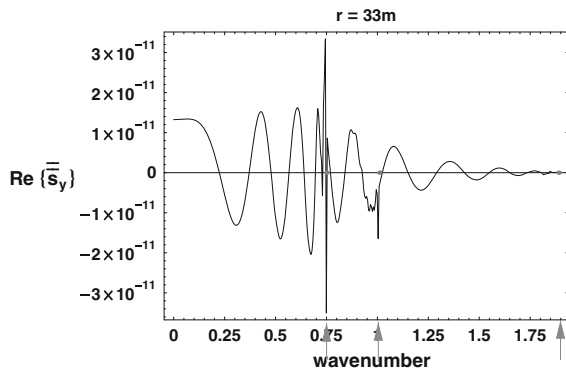
Figure 3

Observations of critical wavenumbers in isotropic medium B from Table 1. The real y component of displacement in the frequency–wavenumber domain is shown at a single field point in a 90 × 90 element system, including a ten element perfectly matched layer. The numerical method used was the spectral element method. Each element is 1 m × 1 m. There are 5 × 5 Gauss–Legendre–Lobatto points per element. The source is real and y-directed. The field point is located 33 m horizontally from the source. The observed critical wavenumbers are 0.97 and 1.57 rad m^{-1} respectively, as indicated in *grey*. The frequency is 300 Hz. There are 500 wavenumbers

Figure 4

Observations of critical wavenumbers in a VTI medium. The real y component of displacement in the frequency–wavenumber domain is shown at a single field point in a 90 × 90 element system, including a ten element perfectly matched layer. The numerical method used was the spectral element method. Each element is 1 m × 1 m. There are 5 × 5 Gauss–Legendre–Lobatto points per element. The source is real and y-directed. The field point is located 33 m vertically below the source. The elastic coefficients are $A_{11} = 6.30$, $A_{13} = 2.25$, $A_{33} = 5.41$, $A_{44} = 1.00$ and $A_{66} = 3.50$. The observed critical wavenumbers are 0.75, 1.01 and 1.89 rad m^{-1}, respectively, as indicated in *grey*. The frequency is 300 Hz. There are 400 wavenumbers

It seems logical that the positions of the critical wavenumbers in a VTI medium would depend on the direction of wave propagation, because the speed of a particular wave mode varies with co-latitude angle. Rather surprisingly, our experiments indicate that the critical wavenumbers have no such directional dependence. Instead they are related to the maximum phase velocities of the medium via the following equations:

$$
\begin{aligned}
(k_y^c)_P &\approx \frac{\omega}{\max\left(\sqrt{\frac{C_{11}}{\rho}}, \sqrt{\frac{C_{33}}{\rho}}\right)} \\
(k_y^c)_{S1} &\approx \frac{\omega}{\sqrt{\frac{C_{44}}{\rho}}} \\
(k_y^c)_{S2} &\approx \frac{\omega}{\sqrt{\frac{C_{66}}{\rho}}}
\end{aligned} \tag{3}
$$

where C_{ij} are the elastic coefficients in reduced Voigt notation.

In fact, the same result is obtained for a tilted transversely isotropic (TTI) medium with a dipping axis of symmetry. Figure 5 demonstrates this lack of directional dependence of the critical wavenumbers by showing the real and imaginary components of the spectrum as a function of k_y for all three components of displacement. The source is x-directed and the axis of symmetry is at 30° to the vertical. The elastic coefficients for this TTI medium are listed in the figure caption. The different colour plots show results for three different receiver positions, at co-latitude angles of 0°, 45° and 90° (all at 9 m distance from the source). The critical wavenumbers, corresponding to the sudden disruptions in the spectra and marked by the yellow arrows, occur at the same positions for all three orientations. Similar results were obtained for y-directed and z-directed sources, also demonstrating a lack of directional dependence.

It eventuates that for more complex anisostropic homogeneous media, the number of critical wavenumbers is given by the number of independent diagonal elements of the Voigt recipe of the 6 × 6 elastic modulus matrix. The maximum number is 6, and is obtained for triclinic symmetry. For orthorhombic symmetry, the number is 4.

In reality, geological media are rarely homogeneous, so in order to develop an applicable wavenumber sampling strategy, some degree of heterogeneity must be introduced. A simple three-layer model was used, as illustrated in Fig. 6. The top and bottom layers have the same material properties, that
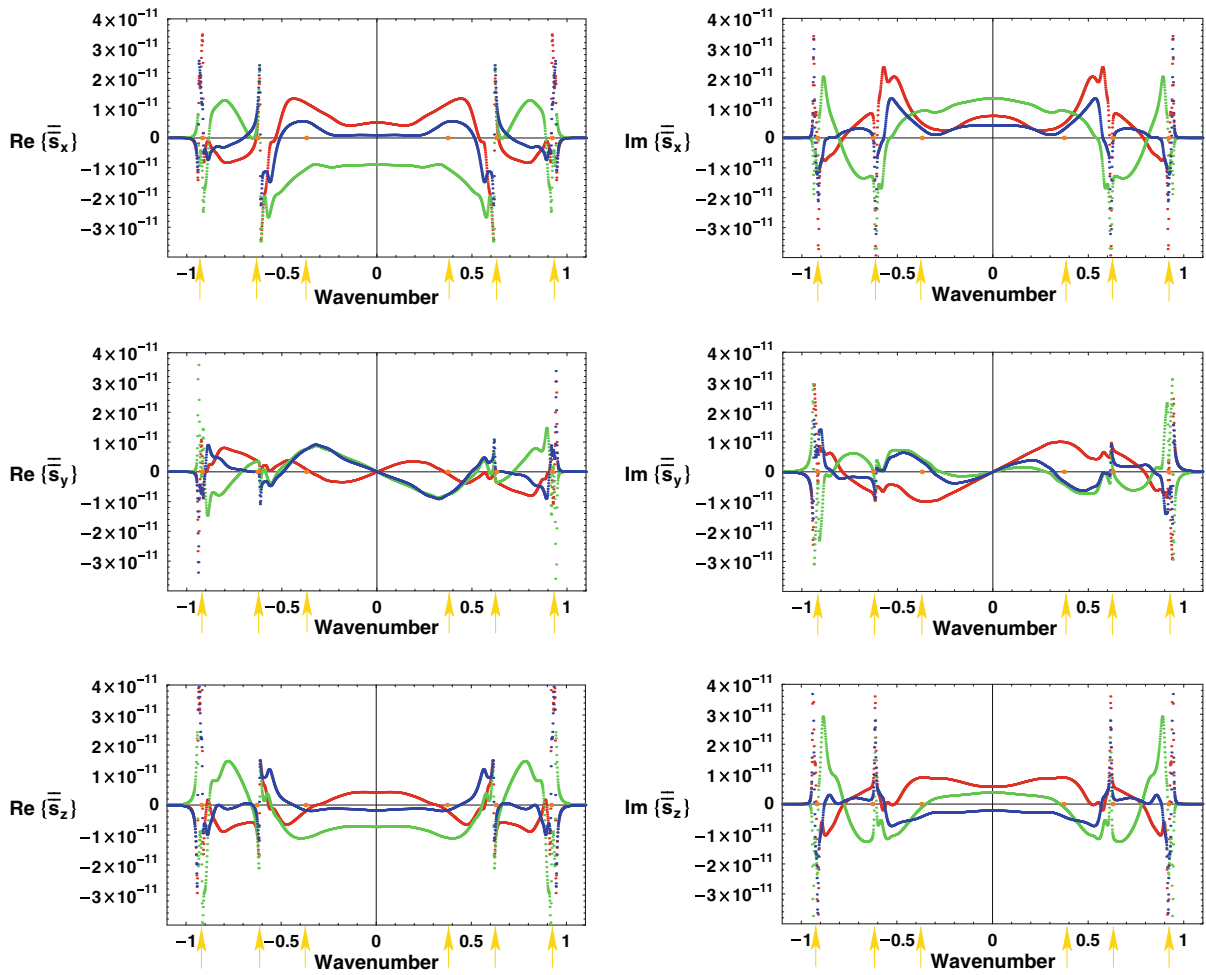
Figure 5

Numerical results show that the critical wavenumbers in a TTI medium at varying propagation directions remain in the same position on the frequency–wavenumber domain plot. The source is real and x-directed. The receivers are placed 9 m from the source, directly below it, at 0° (*red*) and rotating clockwise at 45° (*green*) and at 90° (*blue*). The wavenumbers associated with the maximum phase velocities of the qS1, qS2 and qP wave modes are indicated by the *yellow arrows*. The five independent elastic coefficients in the rock frame are $A_{11} = 25.7$, $A_{13} = 15.2$, $A_{33} = 15.4$, $A_{44} = 4.2$ and $A_{66} = 9.00$. The axis of symmetry is at 30° from the vertical. The frequency is 300 Hz. The numerical method used was the spectral element method. The elements are 1 m × 1 m and there are 5 × 5 Gauss–Legendre–Lobatto points per element. The model includes a ten element wide perfectly matched layer

of medium B in Table 1. The middle layer is a different material (medium A from Table 1) with different critical wavenumbers. The thickness of the middle layer is varied for each experiment from 1 to 6 m. The source is placed in layer 1, at a distance of 1 m above the interface with layer 2. Figure 7 shows the real component of the frequency–wavenumber domain spectra at two receivers, one being placed in the source medium (medium 1) and the other being placed in the lowermost medium (medium 3), with the middle layer (medium 2) in between the two. The

graphed quantity is the y-component of displacement for a y-directed source. The top plots show the results when the middle layer is 1 m thick, the middle plots when the layer is 4 m thick and the bottom plot is for a layer which is 6 m thick.

The effect of the critical wavenumbers in the medium containing the source is filtered out to varying degrees, depending on the thickness of the middle layer. The thicker the layer, the greater the filtering effect. In other words, the disruptions in the spectra become less pronounced as the thickness of
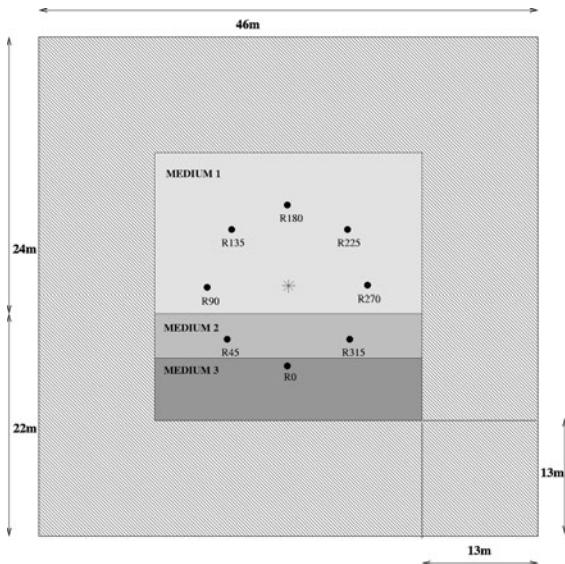
Figure 6

A simple inhomogeneous model with three layers, 46 m × 46 m. The source, shown by the star, is in the centre within medium 1, at a distance of 1 m from the interface between medium 1 and medium 2. The thickness of medium 2 varies during the experiment. Receivers R0 and R180 are at a radii of 9 m, but in opposite directions from the source. The model has a 13 m thick absorbing layer on all four edges so the area of interest is only 20 m × 20 m

the intermediate layer increases. By repeating the experiment on various isotropic media we have observed that the highest degree of filtering is obtained if the thickness of the intermediate layer is at least one P-wave wavelength of the medium containing the source. In the case of the experiment described in Fig. 7, the P-wavelength of medium B for a frequency of 300 Hz is 6.5 m.

Another phenomenon is observable in Fig. 7. As the intermediate layer becomes thicker, two additional critical wavenumbers become apparent at wavenumbers of approximately $k_y = 1.67$ rad m^{-1} and $k_y = 1.82$ rad m^{-1}. These critical wavenumbers do not correspond with the P and S critical wavenumbers of medium B or medium A (see Table 1). The disruptions become more pronounced the thicker the layer. It is likely that these critical wavenumbers are associated with Stoneley waves that propagate in the vicinity of the interface between the two media. Referring to the model depicted in Fig. 6, as the middle layer is made thicker, the interface comes into closer proximity with the receiver, and hence the

receiver detects the Stoneley waves to a greater degree.

4. The Effect of Critical Wavenumbers on the Frequency Domain Solution

As demonstrated above, critical wavenumbers are observable in the frequency–wavenumber domain solutions as disruptions in the mainly smooth, oscillatory curves. Sometimes the amplitudes of the disruptions are very large and affect the accuracy of the inverse Fourier transformed frequency-space domain solution.

Figure 8 compares the isotropic analytic solution from AKI and RICHARDS (1980) with the numeric solution which is produced via an inverse Fourier transformed summation from 32 individual frequency–wavenumber domain solutions. The match is very poor. The overall amplitude of the numeric solution is artificially boosted because the sample closest to the S-wave critical wavenumber of 1.57 rad m^{-1} has a very large amplitude. Figure 9 illustrates this fact by showing the frequency–wavenumber domain spectrum at a single point in space, 8 m from the source. Each stem is the numeric solution at that point for a particular wavenumber. The spectral amplitude at wavenumber 1.57 rad m^{-1} is significantly larger than other amplitudes. Because all samples carry the same weighting in the inverse Fourier transform summation, the final 2.5D solution has a larger than expected magnitude (see Fig. 8, where the numerical curve lies above the analytic curve). It is also noted that the neighbouring part of the spectral curve that oscillates in the negative direction is not sampled, compounding the problem, because a sample in this region would counteract the effect of the large positive amplitude sample. Obviously, a finer wavenumber interval and more samples would mitigate the problem.

5. Removal of Singularities by the Introduction of Slight Attenuation

It is important to establish if there are poles (singularities) in the numerical solutions because if a
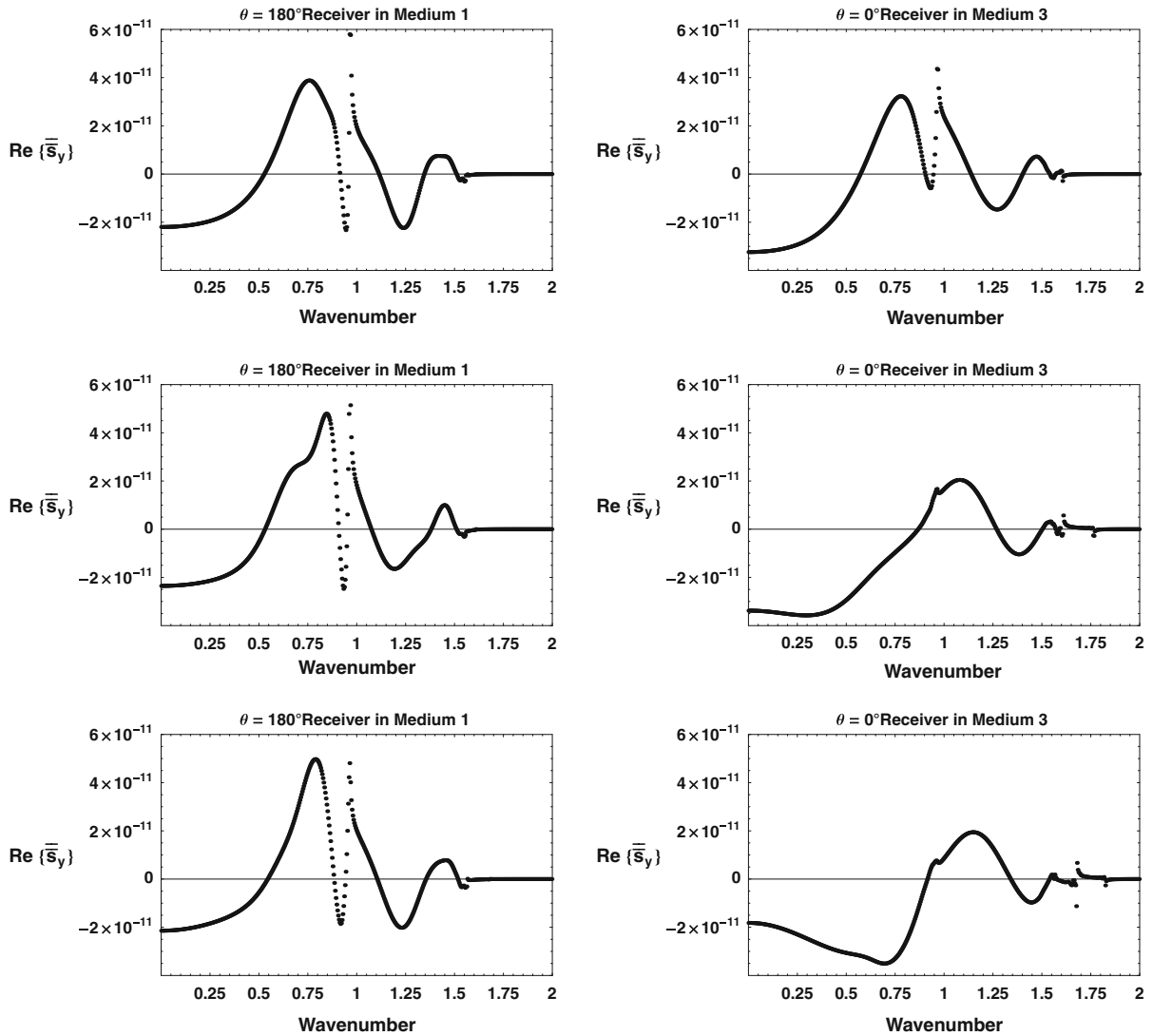
Figure 7

Critical wavenumbers in a simple three-layer inhomogeneous model. The real y component of the solution in the frequency–wavenumber domain is shown for a y-directed source in the 46 m × 46 m model shown in Fig. 6. Medium 1 = B, medium 2 = A, medium 3 = B with medium properties as described in Table 1. The source is in medium B. The receiver is at a radius of 9 m, directly below the source at 0° (position R0 within medium 3) and directly above the source at 180° (position R180 within medium 1). The plots on the *left* show the spectra for a receiver located in medium 1. The plots on the *right* show the spectra for a receiver located in medium 3. The thickness of medium 2 is 1 m for the top plots, 4 m for the middle plots and 6 m for the bottom plots. The numerical method used was the spectral element method. The elements are 1 m × 1 m and there are 5 × 5 Gauss–Legendre–Lobatto points per element

wavenumber sample coincided with a pole, the amplitude of the inverse Fourier transformed solution would be far too high. In the Fourier transformed analytic solution, as the spacing between samples decreases, the amplitude of the particle displacement increases rapidly with increasing proximity to the critical wavenumber, suggestive of poles. In

comparison, the 2.5D numerical solution produced using the spectral element method, is bounded. This is clearly shown in Fig. 10, where the equations of motion are solved at 2,048 wavenumbers within a region very close to the P-wave critical wavenumber. In this case, at 300 Hz, the critical wavenumber is: $(2\pi \times 300)/1,950 = 0.967$ rad m^{-1}. Using finer and
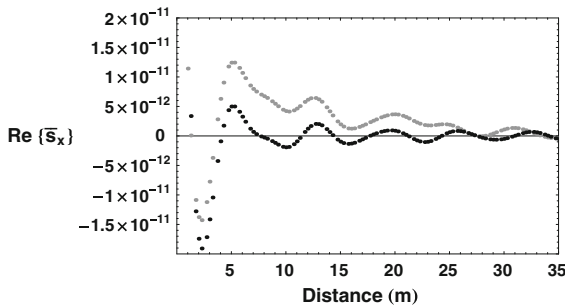
Figure 8

The two curves show the real x component of the solution using a real *x*-directed source. The *grey* curve shows the inverse Fourier transformed numeric solution constructed from 32 wavenumber samples. The *black* curve shows the analytic solution. The medium is homogeneous isotropic medium B from Table 1. The frequency is 300 Hz. The absorbing boundaries are 10 m wide. The numerical method used was the spectral element method. The elements are 1 m × 1 m and there are 5 × 5 Gauss–Legendre–Lobatto points per element
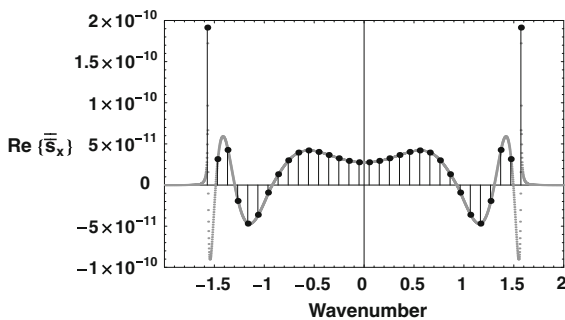

Figure 9

A wavenumber sample is taken close to the critical wavenumber at 1.571 rad m^{-1}. The *grey* curve shows the Fourier transformed analytic solution for the real x component in the plane containing the source, using a real *x*-directed source. The stem plot shows the numerical solution calculated at 32 evenly spaced wavenumbers using the spectral element method. The elements are 1 m × 1 m and there are 5 × 5 Gauss–Legendre–Lobatto points per element. The receiver is 8 m from the source. The frequency is 300 Hz. The medium is homogeneous isotropic medium B from Table 1. The absorbing boundaries are 10 m wide

finer sample spacings did not change the curve. The discrepancy between the numerical and analytic results is likely to be linked to the numerical formulation itself. In the spectral element method we use the weak form of solution of the equations of motion and estimate spatial derivatives using a limited number of surrounding quadrature points, which offers an approximate solution. It is unknown (but most unlikely) that other numerical methods would

produce pole-like behaviour. Nevertheless, we need to investigate a method that avoids the problems associated with poles.

It has been shown theoretically by means of analytic solutions (SINCLAIR 2009) that the singularities existing in the 2.5D solutions can be removed via the addition of a small imaginary part to either the velocities or the elastic moduli. This introduces a slight attenuation and moves the critical wavenumbers off the real axis along which the wavenumber summation (the inverse Fourier transform) is performed. In this way it is ensured that the wavenumber sample does not directly fall on a pole. The attenuation is kept sufficiently small so as to not distort the wavefield solution. The use of complex frequency, as discussed by CAO and GREENHALGH (1997) and BOUCHON (2003), achieves a similar result, but in that case a positive exponential time function is applied after the inverse temporal Fourier transform, to compensate the effect.

The implementation for 2.5D numerical modelling of elastic waves would need to accommodate complex elastic moduli, effectively making the technique a visco-elastic modelling scheme. An example is given in a later section..
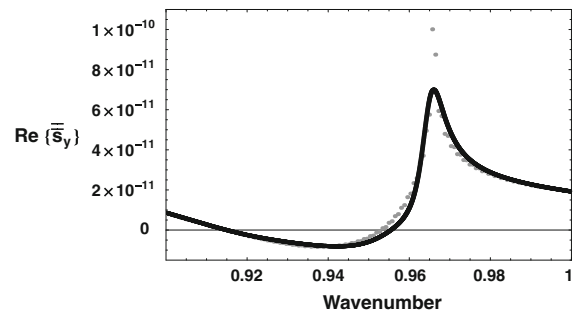

Figure 10

The *grey curve* shows the Fourier transformed analytic solution, zoomed into the wavenumber range of interest. The behaviour is consistent with a pole. The *black curve* shows the numeric solution calculated using the spectral element method at 2,048 wavenumber samples between 0.9 and 1.0 rad m^{-1}. The elements are 1 m × 1 m and there are 5 × 5 Gauss–Legendre–Lobatto points per element. The numeric solution is bounded. The source is real and y-directed. Only the real y component of the solution is shown. The receiver is 9 m directly below the source. The medium is homogeneous isotropic medium B from Table 1. The frequency is 300 Hz

6. A Suggested Wavenumber Sampling Strategy

Our experiments have shown that, although the behaviour of the 2.5D wavefields close to the critical wavenumbers is erratic, some aspect of that behaviour needs to be adequately captured to yield reliable spatial-domain solutions. The simplest way to achieve this is to use finely spaced wavenumber samples. It is difficult to determine the exact number of wavenumbers required for a given level of accuracy because different factors affect it, including the direction of the source, the distance from the source, the frequency and the elastic coefficients of the medium. A suggested approach is to experiment by increasing the number of wavenumbers until further increases do not change the inverse Fourier transformed solution to a significant degree. Figure 11 illustrates the improvement in relative error of the inverse Fourier transformed solution against the analytic solution, when the number of 2.5D wavenumber solutions is increased from 32 to 128. The errors decrease from 5.8 to 0.2%.

One could always oversample in wavenumber at some very fine equal interval, as STREICH and van der KRUK (2007) did in eliminating the effects of antenna radiation/reception patterns in ground penetrating radar imaging. They oversampled by a factor of 4–16 relative to the Shannon criterion, but they had analytic solutions to use for the ω-k domain Green's functions. They did not have to solve a finite difference or finite element system of linear equations for every wavenumber (and every frequency), as arises in 2.5D frequency domain seismic modelling. As is so often the case in geophysics, there is a trade-off between accuracy and computational efficiency.

7. A 2D Anisotropic Example : Frequency Domain Wavefields

Figure 12 shows a two-layered anisotropic (VTI) model having an anomalous block of the lower layer material embedded in layer 1. The densities and elastic constants for the two solids are given in the figure. We have calculated the frequency domain wavefields (at a frequency of 100 Hz) in the central plane for all non-zero components of the Green's
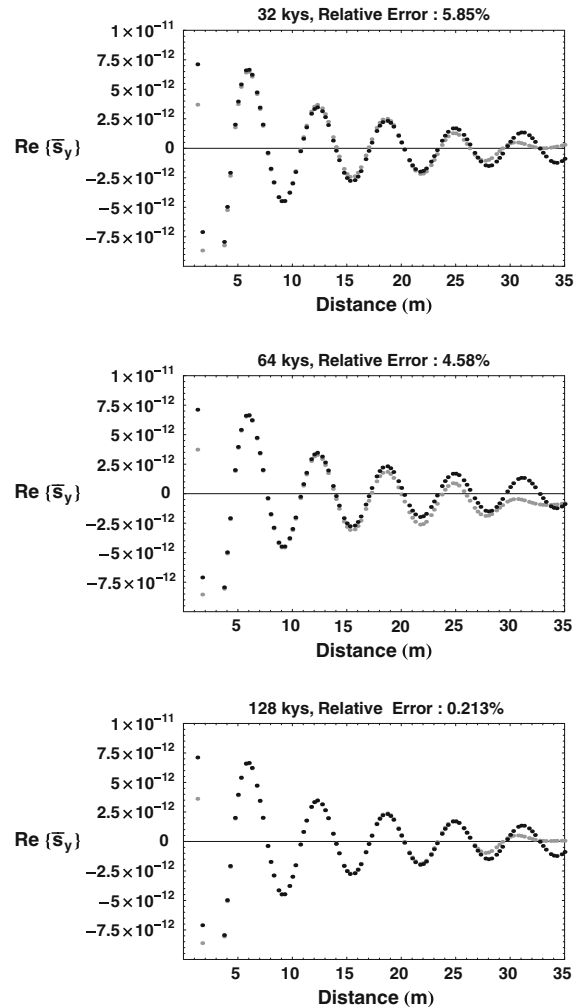

Figure 11

In each plot, the two curves show the real y component of the solution using a real *y*-directed source. The *grey curve* shows the inverse Fourier transformed numeric solution constructed from 32, 64 and 128 wavenumber solutions. The *black curve* shows the analytic solution. The cross section is in a horizontal direction in the plane containing the source. The elastic coefficients of the homogeneous VTI medium are $A_{11} = 6.30$, $A_{13} = 4.30$, $A_{33} = 6.30$, $A_{44} = 1.00$ and $A_{66} = 3.50$. There are only three independent elastic coefficients. The frequency is 300 Hz. The relative errors are calculated at the local maximum at 12.28 m. The absorbing boundaries are 10 m wide, starting at 25 m from the source. The numerical method used was the spectral element method. The elements are 1 m × 1 m and there are 5 × 5 Gauss–Legendre–Lobatto points per element

function tensor (G_{11}, G_{13}, G_{22}, G_{31}, G_{33}), where the first subscript on G denotes the source direction and the second subscript the receiver direction. The source is located on the surface at horizontal position 0. The frequency domain solution was obtained by

summing the wavenumber spectra for 125 wavenumbers from 0 out to the highest critical wavenumber in the model. A small value ($\varepsilon = 10^{-12}$) was assigned to the diagonal elements of the elasticity tensor to damp out the singularities at the critical wavenumbers. For each VTI medium there are three critical wavenumbers, giving rise to six in total at a frequency of 100 Hz. The frequency domain results are shown (both real and imaginary parts) in Fig. 12. Note that the G_{13} wavefield is different to the

G_{31} wavefield because of the 2D heterogeneous nature of the model. The Green's function components G_{12}, G_{21}, G_{23} and G_{32} are each zero because motion is depicted in the central plane and a source in the y-direction (perpendicular to the page) cannot produce displacements in the z- or x-directions within this plane. Similarly, a z- or x-directed source cannot produce motion in the y-direction within the central plane. The wavefield patterns are rather complicated but show the oscillatory nature of the disturbance and
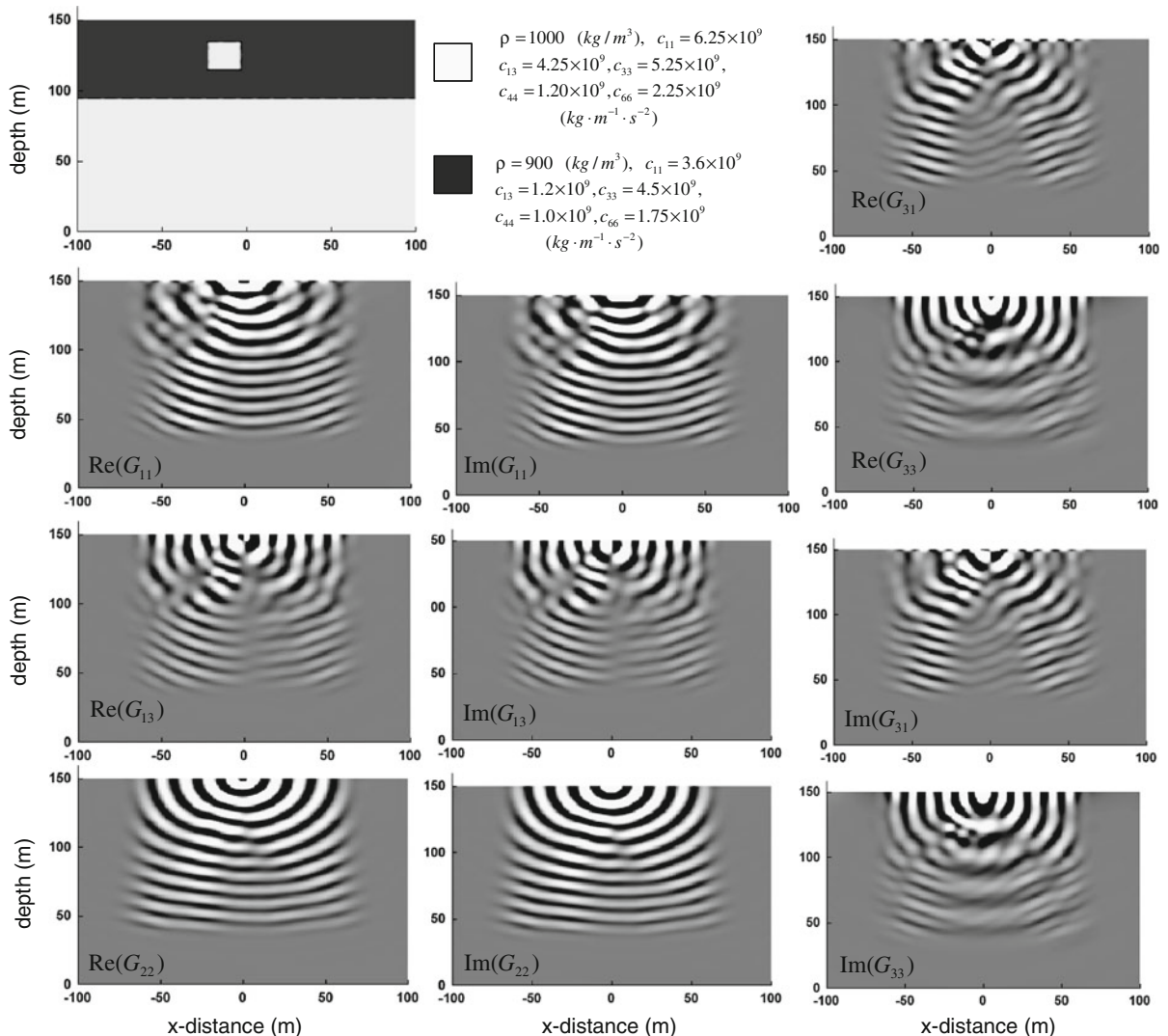

Figure 12

Real and imaginary parts of the Green's tensor components G_{11}, G_{13}, G_{22}, G_{31} and G_{33}, showing the frequency domain wavefield at 100 Hz for the 2D anisotropic model (shown in *upper left*) comprising two VTI layers with an anomalous block of the lower layer embedded in layer 1. The density and elastic moduli values for each layer are given in the *upper middle* part of the figure. The source is located at position (0, 150)
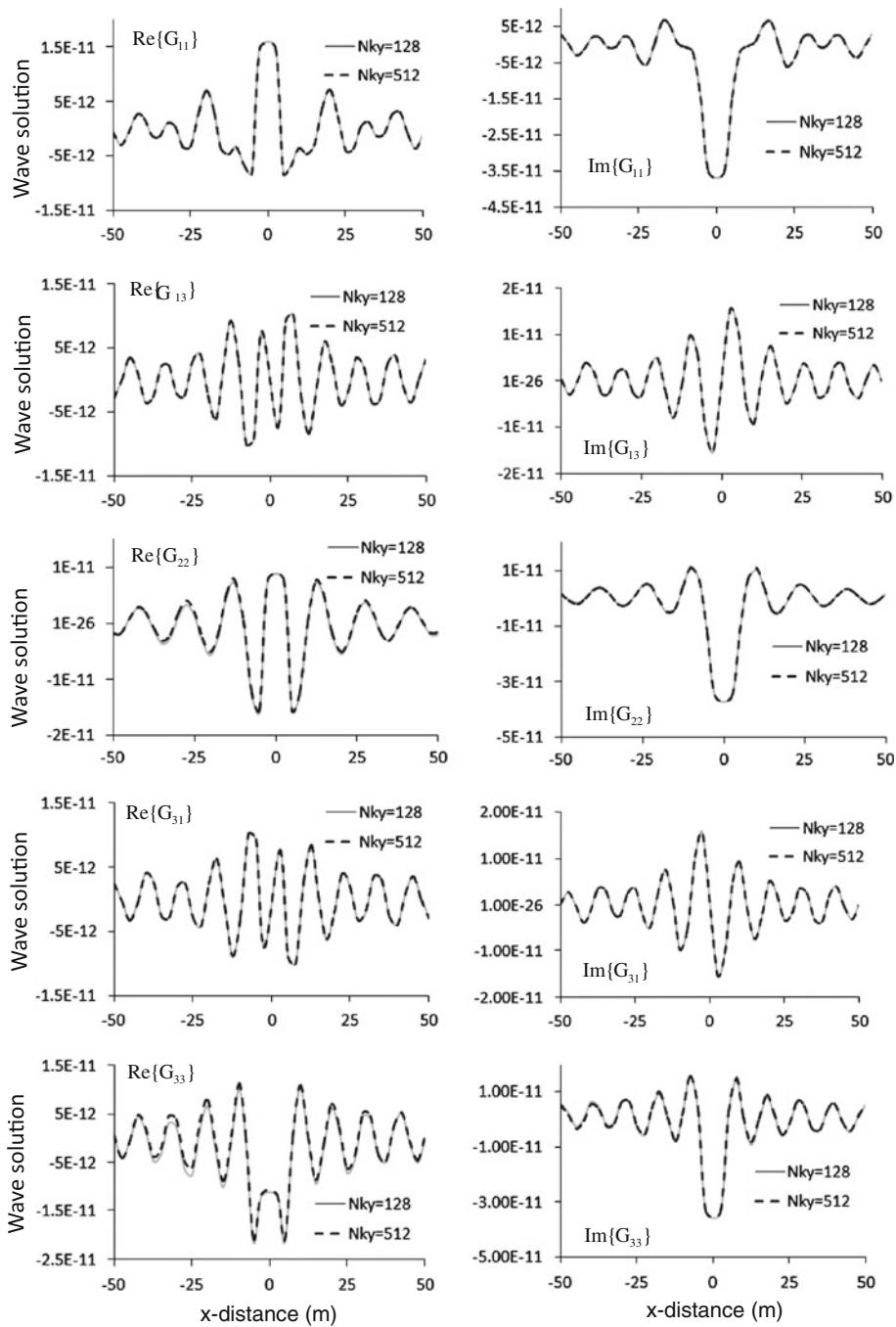
Figure 13

Green's tensor solutions (real and imaginary parts) at 100 Hz as a function of distance along the top surface of the model shown in Fig. 12. Results are displayed for two sets of wavenumber spectra: $N_{ky} = 128$ and $N_{ky} = 512$. The larger number of k_y values is expected to yield a more accurate result but the curves for the two cases track each other very closely for all tensor components. This indicates that the sampling strategy used, combined with slight attenuation to damp out the singularities at the critical wavenumbers, is a satisfactory approach for 2.5D frequency domain modelling

the reflections arising from the layer boundary and the square inclusion.

Figure 13 shows the solutions as a function of distance along the top surface of the model. The plot includes the real and imaginary parts of the frequency domain solution for all five components of the Green's function tensor. Results are given for two different numbers of wavenumber spectra: $N_{ky} = 128$ and $N_{ky} = 512$. The latter is expected to give a more accurate result but it is clear from the plots that the two sets of curves track each other almost identically. Note that the Green's function components G_{11}, G_{22}, G_{33} all exhibit even symmetry about the source position whereas the components G_{13}, G_{31} show odd symmetry. This suggests that some economies can be achieved with the wavenumber spectra by only working with positive wavenumbers and imposing the symmetry condition on the negative wavenumbers.

8. Conclusions

We have shown that there are critical wavenumbers associated with each of the wave modes in 2.5D elastic wave modelling. Our investigations revealed that in tilted transversely isotropic (TTI) media, the position of a critical wavenumber along the wavenumber axis is independent of propagation direction. We have demonstrated that erratic behaviour close to critical wavenumbers in the 2.5D frequency–wavenumber domain spectra can seriously compromise the accuracy of the inverse Fourier transformed frequency domain solution, particularly if an insufficient number of wavenumber samples are taken. We suggest that a large number of equi-spaced wavenumber samples should be used to construct the frequency domain solution, thereby ensuring that the erratic behaviour close to the critical wavenumbers is adequately captured. Although our numerical results do not contain poles, we consider it wise to remove any possible singularities by introducing a slight attenuation to the elastic coefficients. The results from our experiments in simple heterogeneous media have implied benefits for wavenumber sampling. Preliminary observations indicate that intermediate layers between the source and receiver locations can filter out the disruptions in the wavenumber

behaviour and that the problems associated with critical wavenumbers only need to be considered for receivers within the medium containing the source. This is with the proviso that the intermediate medium does not share critical wavenumbers with the source medium. To effectively suppress the effects of the critical wavenumbers in isotropic media, we found that the thickness of the intermediate medium must be at least one P-wave wavelength of the source medium.

References

AKI, K., and RICHARDS, G., Quantitative Seismology Theory and Methods, Vol I,II (W.H. Freeman and Company, San Francisco 1980).

BLEISTEIN, N. (1986), *Two-and-one-half dimensional in-plane wave propagation*, Geophysical Prospecting *34*, 686-703.

BOUCHON, M. (2003), *A review of the discrete wavenumber method*, Pure Appl. Geophys. *160*, 445-465.

BOUCHON, M. (1996), *The discrete wavenumber formulation of boundary integral equations and boundary element methods: A review with applications to the simulation of seismic wave propagation in complex geological structures*, Pure Appl. Geophys. *148*, 3-20.

CAO, S. and GREENHALGH, S.A. (1997), *2.5-D acoustic wave modelling in the frequency-wavenumber domain*, Expl. Geophys. *28*, 11-15.

CAO, S. and GREENHALGH, S.A. (1998), *2.5-D modelling of seismic wave propagation : Boundary condition, stability criterion, and efficiency*, Geophysics *63*, 2082-2090.

CARCIONE, J.M., Wave Fields in Real Media: Wave Propagation in Anisotropic, Anelastic, Porous and Electromagnetic Media, Handbook of Geophysical Exploration, Seismic Exploration, vol.38 (Second edition, Revised and Extended) (ed. Helbig K. and Treitel S.) (Elsevier, Oxford, UK-Amsterdam, The Netherlands 2007).

CHOI Y., MIN., D., and CHANGSOO, S. (2008), *Two-dimensional waveform inversion of multi-component data in acoustic-elastic coupled media*, Geophysical Prospecting *56*, 863-881.

ERNST, J., MAURER, H., GREEN, A., and HOLLIGER, K. (2007), *Full waveform inversion of cross-hole radar data based on 2D finite difference time domain solution of Maxwell's equations*, IEEE Trans. Geosci. and Remote Sensing *45*, 2807-2828.

EWING, W.M., JARDETZKY, W.S. and PRESS, F., Elastic Waves in Layered Media (Mc Graw Hill, New York 1957).

FUJIWARA, H. (1996). *Three-dimensional wavefield in a two-dimensional basin structure due to a point source*, J. Phys. Earth *44*, 1-22.

FUJIWARA, H. 1997. *Windowed f-k spectra of a three-dimensional wavefield excited by a point source in a two-dimensional multi-layered elastic medium*: Geophy. J. Int. *128*, 571-584.

FURUMURA, T., and TAKENAKA, H. (1996), *2.5-D modelling of elastic waves using the pseudo-spectral method*, Geophys. J. Internat., *124*, 820-832.

KOMATITSCH, D., BARNES, C., and TROMP, J. (2000), *Simulation of anisotropic wave propagation based upon a spectral element method*, Geophysics, *65*, 1251-1260.

KELLY, K.R. and MARFURT, K.J. 1990 (Eds). Numerical Modelling of Seismic wave Propagation: Society of Exploration Geophysicists, Tulsa, Geophysical Reprint Series, 519 pp.

LINER, C. (1991), *Theory of a 2.5-D acoustic wave equation for constant density media*, Geophysics *56*, 2114-2117.

MARFURT, K. (1984), *Accuracy of finite-difference and finite-element modelling of the scalar and elastic wave equations*, Geophysics *49*, 533-549.

MAURER, H., GREENHALGH, S., and LATZEL, S. (2009), *Frequency and spatial sampling strategies for crosshole seismic waveform spectral inversion experiments*, Geophysics *74*, WCC79-WCC89.

OKAMOTO, T. (1994), *Teleseismic synthetics obtained from 3-D calculation sin 2-D media*, Geophys. J. Int. *118*, 613-622.

PRATT, R. (1990), *Frequency-domain elastic wave modelling by finite differences: A tool for crosshole seismic imaging*, Geophysics *55*, 626-632.

RANDALL, C.J. 1991. *Multipole acoustic waveforms in nonaxisymmetric boreholes and formations*: J. Acoust. Soc. Am. *90*(3), 1620-1631.

ROBERTS, M., SINGH, S., and HORNBY, B. (2008), *Investigation into the use of 2D elastic wave-form inversion from look-ahead walkaway VSP surveys*, Geophysical Prospecting *56*, 883-895.

SEARS, T., SINGH, S., and BARTON, P. (2008), *Elastic full waveform inversion of multi-component OBC seismic data*, Geophysical Prospecting *56*, 843-862.

SINCLAIR, C. (2009), Elastic wave modelling in anisotropic media using the spectral-element method, Ph.D. thesis, University of Adelaide, Australia.

SINCLAIR, C., GREENHALGH, S., and ZHOU, B. (2007), *2.5D modelling of elastic waves in transversely isotropic media using the spectral element method*, Expl. Geophys. *38*, 225-234.

SONG, Z., and WILLIAMSON, P. (1995), *Frequency-domain acoustic wave modelling and inversion of crosshole data: Part I – 2.5- D modelling method*, Geophysics *60*, 784-795.

STOCKWELL, J.W., JR. (1995), *2.5-D wave equations and high frequency asymptotics*, Geophysics *60*, 556-562.

STREICH, R. and van der KRUK, J. (2007), *Accurate imaging of multicomponnet GPR data based on exact radiation patterns*, IEEE Trans. Geosci. And Remote Sensing *45*, 93-100.

TADEU, A., and KAUSEL, E. (2000), *Green's functions for two-and-a-half-dimensional elastodynamic problems*, Journal of Engineering Mechanics *126*, 1093-1097.

TANENAKA, H., KENNETT, B.L.N. and FUJIWARA, H. 1996. *Effect of 2-D topography on the 3-D seismic wavefiled uisng a 2.5-D discrete wavenumber – boundary integral equation method*: Geophys. J. Int. *124*, 741-755.

WILLIAMSON, P., and PRATT, R. (1995), *A critical review of acoustic wave modelling procedures in 2.5 dimensions*, Geophysics *60*, 591-595.

YANG, Y., and HUNG, H. (2001), *A 2.5D finite/infinite element approach for modelling visco-elastic bodies subject to moving loads*, International Journal for Numerical Methods in Engineering *51*, 1317-1336.

ZHOU, B., and GREENHALGH, S. (1998a), *Composite boundary-valued solution of the 2.5-D Green's function for arbitrary acoustic media*, Geophysics *63*, 1813-1823.

ZHOU, B., and GREENHALGH, S. (1998b), *A damping method for the computation of the 2.5-D Green's function for arbitrary acoustic media*, Geophys. J. Internat. *133*, 111-120.

ZHOU, B., and GREENHALGH, S. (2006), *An adaptive wavenumber sampling strategy for 2.5D seismic wave modelling in the frequency domain*, Pure Appl. Geophys. *163*, 1399-1416.